Eur. J. Mineral.
2011, **23**, 179–196
Published online January 2011

# Serpentine and chlorite as effective Ni-Cu sinks during weathering of the Aguablanca sulphide deposit (SW Spain). TEM evidence for metal-retention mechanisms in sheet silicates

SAIOA SUÁREZ[1,*], FERNANDO NIETO[2], FRANCISCO VELASCO[1] and FRANCISCO J. MARTÍN[3]

[1] Departamento de Mineralogía y Petrología, Universidad del País Vasco, 48940 Lejona, Vizcaya, Spain
*Corresponding author, e-mail: saioa.suarez@ehu.es
[2] Instituto Andaluz de Ciencias de la Tierra y Departamento de Mineralogía y Petrología, Universidad de Granada-CSIC, 18002 Granada, Spain
[3] Departamento de Edafología y Química Agrícola, Universidad de Granada, 18002 Granada, Spain

**Abstract:** Supergene alteration in the Aguablanca Ni-Cu-(PGE, platinum group elements) magmatic sulphide deposit (SW Spain) has formed distinctive soil profiles overlying the gabbroic host rocks. These profiles have subsurficial clayey horizons exceptionally enriched in Ni and Cu even in areas distant from the orebodies and the related gossan outcrops. A preliminary study of the mineralogy in these profiles including bulk analyses by electron microprobe (EMP) and energy dispersive X-ray spectrometry (EDS), showed that outstanding base-metal contents are retained by sheet silicates. Lizardite and clinochlore are the most remarkable Ni and Cu scavengers (up to 44 wt% NiO and 9 wt% CuO), with smectite, vermiculite and corrensite playing a subordinate role in this retention (up to 4 wt% NiO and 3 wt% CuO). These results suggest that Ni and Cu could be within the structure of these sheet silicates, but transmission electron microscopy (TEM) imaging has revealed that Ni, and especially Cu, also occur as discrete metallic particles. Notable differences are detected in the redistribution of base-metals among the major carriers after sulphides dissolution in supergene conditions. Copper is largely retained as native particles in sheet-silicates, particularly in chlorite, whereas Ni is largely bound to the structure, especially in serpentine. This reflects variable metal-retention mechanisms by sheet silicates at Aguablanca, related not only to the host phases but also to the low-temperature conditions in the deposit. Detailed analysis and imaging of the individual Ni-Cu-bearing phases were used to evaluate these retention processes.

**Key-words:** chlorite, lizardite, nepouite, native Cu particles, Ni-(Fe ± Cu) particles, HRTEM, Aguablanca.

## Introduction

Fine-grained minerals may play a significant role in retaining heavy metals during the exogenic cycle in base-metal deposits. Iron- and Mn-oxides and hydroxides are highly reactive minerals and well-known scavengers of heavy metals at the surface of such deposits (Thornber & Wildman, 1984; Manceau *et al.*, 1992; Cornell & Schwertmann, 1996). However, in lower parts of profiles, where illuviation may be intense and oxides are not as developed, sheet silicates influence this retention heavily due to their large sorption capacity (*e.g.*, Koppelman & Dillard, 1977; Dinelli & Tateo, 2001; Gustafsson, 2004).

Clay-rich horizons and fissures cross-cutting the subsurficial weathering profiles of the Aguablanca deposit accommodate extensive Ni- and Cu-bearing phyllosilicates. The base-metal contents of the serpentine and chlorite in this deposit are comparable to the high-grade Ni- and Cu-sheet silicates, respectively, reported in deposits subjected to strong lateritization and oxidation processes. Nickel-bearing sheet silicates have been widely investigated in laterites from Brazil (Colin *et al.*, 1990; Barros de Oliveira *et al.*, 1992), Ivory Coast (Nahon *et al.*, 1982; Noack & Colin, 1986), New Caledonia (Trescases, 1975; Pelletier, 1996; Wells *et al.*, 2009) and Western Australia (Elias *et al.*, 1981), amongst others. Anomalous copper concentration in sheet silicates are mainly reported in rocks associated with porphyry copper deposits, like those from North America and the Solomon Islands (*e.g.*, Hendry *et al.*, 1981; Ilton & Veblen, 1988, 1993; Ahn *et al.*, 1997). The characterization of these types of clay minerals has long been of interest to estimate their potential utilization, and elucidate the mode and timing of their metal enrichment.

This work evaluates the metal-retention processes undergone by clay minerals in a supergene Ni-rich, but also Cu-rich, low-temperature environment. The main objectives were to: (i) characterize the main Ni-Cu-bearing phases and assess their suitability as metal traps, (ii) estimate the mechanisms for their selective base-metal retention,

DOI: 10.1127/0935-1221/2011/0023-2084
0935-1221/11/0023-2084 $ 8.10

and (iii) evaluate the geochemical controls allowing this retention. The combined study using several electron microscope techniques, including high-resolution transmission electron microscopy (HRTEM), provides an insight into the Ni and Cu sequestration by sheet silicates in a natural environment of the subsurface of a Ni-Cu-sulphide deposit.

## Geological background

Aguablanca is an orthomagmatic Ni-Cu-(PGE) sulphide deposit located in Extremadura, SW Spain. It is situated in the southern limb of the Olivenza-Monesterio Antiform, a major Variscan structure of the Ossa Morena Zone, and belongs to the Santa Olalla Plutonic Complex (Fig. 1). The deposit consists of two sub-vertical, ellipsoidal pipe-like orebodies (E-W, 80°N) hosted by the small Aguablanca Stock. This stock is a heterogeneous calc-alkaline Variscan intrusion formed by diorite and quartz diorite (*Dioritic Unit*), and gabbronorite, norite and melanocratic pyroxene gabbro (*Gabbronorite Unit*) (Casquet *et al.*, 2001; Tornos *et al.*, 2001; Romeo *et al.*, 2006). The complex is hosted by Late Proterozoic to Early Cambrian dark shales (*Serie Negra*, Quesada *et al.*, 1987), limestones, volcanic rocks and sandstones that underwent high-grade contact metamorphism (Velasco, 1976; Casquet, 1980).

The mineralization is dominated by pyrrhotite, pentlandite and chalcopyrite with subordinate magnetite and pyrite, and a great deal of accessory minerals including platinum-group minerals (Ortega *et al.*, 2004; Piña *et al.*, 2008; Suárez *et al.*, 2010). The ore occurs as semi-massive sulphide-supported breccias, minor lenses of massive sulphides and, mostly, as disseminations within the *Gabbronorite Unit*. Mineralization in patches or veinlets occurs in distal parts of the deposit, towards the barren lithologies (*Contact Gabbro*; Tornos *et al.*, 2006). Proven and probable reserves in the main mineralization zones are 15.7Mt@0.66 % Ni, 0.46 % Cu, 0.47 g/t PGE and 0.13 g/t Au (Río Narcea Recursos S.A.-Lunding Mining Corporation, 2009).

Post-magmatic evolution of the deposit includes pervasive polyphase hydrothermalism that transformed primary igneous silicates and gave rise to irregular masses and veinlets including phlogopite, amphibole, epidote, feldspars, chlorite, talc, phengite, quartz, calcite, and sulphides (Ortega *et al.*, 2004; Tornos *et al.*, 2006). Subsequent supergene alteration has formed irregular outcrops of about 8 m thick-goethitic gossan restricted to shallow parts of the deposit where massive to semi-massive mineralization occurs. Towards the surrounding lower-grade areas, a strong weathering front spreads out to form poorly oxidized soil horizons over the host gabbroic lithologies, where the present study is focussed.

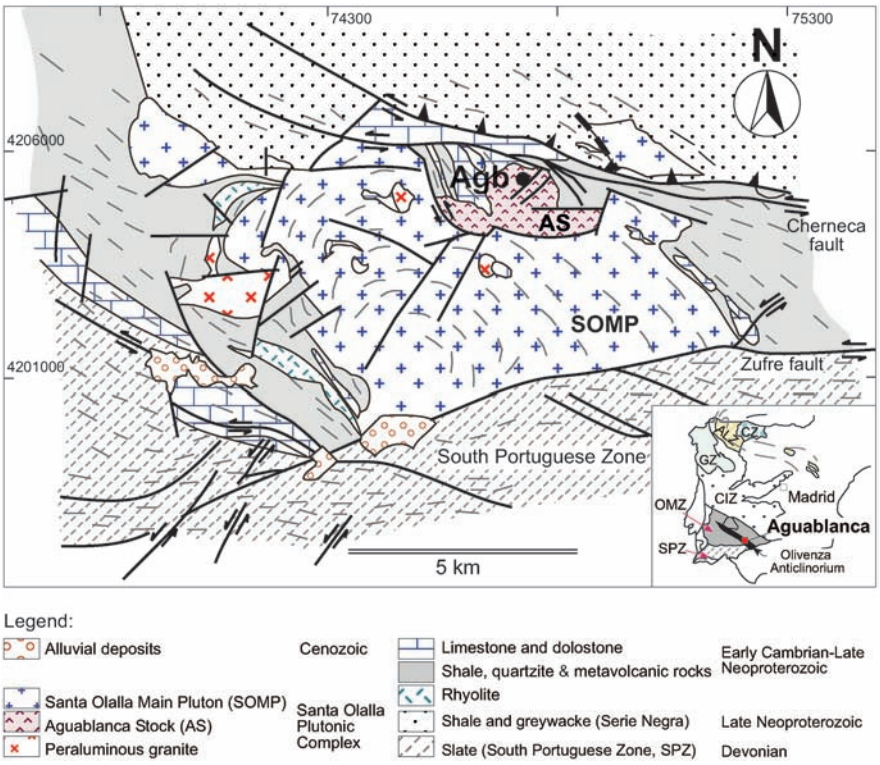


Fig. 1. Geological map of the Santa Olalla Plutonic Complex showing the Aguablanca mine site. Modified from Casquet (1980). The inset box shows the Variscan chain division in the Iberian Massif.
Note: *Agb*, Aguablanca Mine; *ALZ*, Asturian Leonese Zone; *AS*, Aguablanca Stock; *CZ*, Cantabrian Zone; *CIZ*, Central Iberian Zone; *GZ*, Galicia Tras-Os-Montes Zone; *OMZ*, Ossa Morena Zone; *SPZ*, South Portuguese Zone.

## Materials and methods

Eight weathering profiles surrounding the orebodies and exposed during the operations at the Aguablanca mine site were sampled from the unaltered host gabbro to the upper soil horizons. Five of these profiles belong to ore-grade areas of the *Gabbronorite Unit* ($n = 44$ samples) and the other three profiles ($n = 20$ samples) belong to low-grade and barren areas of the *Contact Gabbro*, where the cut-off grade is <0.2 wt% NiO.

The physicochemical properties of the weathered horizons were analyzed in the <2 mm fraction following the standard methods of soil analysis described in Marañés *et al.* (1998). The geochemistry of the profiles was analyzed by X-ray fluorescence (XRF) using a Philips 1480 wavelength dispersive spectrometer. The mineralogy was investigated in thin sections and by X-ray diffraction (XRD) using a Philips PW1710 powder diffractometer with Cu-$K\alpha$ radiation in both the <2 mm and <2 μm fractions, the latter obtained by sedimentation and prepared on glass slides. Ethylene glycol, dimethyl sulfoxide, and heat treatments were carried out on the orientated aggregates. Amberlite IR-200 ion-exchange resin was used to homoionize with $Li^+$, $K^+$ and $Mg^{2+}$. Metallic Si was used as a standard, and the relative mineral abundance was calculated according to Schultz (1964). The exchangeable fraction was extracted from 16 selected clayey samples by saturation with ammonium acetate 1N at pH = 7, after removal of the water-soluble fraction. Metal concentrations in the former fraction were analyzed using a Perkin Elmer 305B atomic absorption spectrophotometer.

Representative thin sections of the soil horizons were analyzed using a Cameca-MBX and a Jeol JMS 6400 electron microprobes (accelerating voltage of 15 kV, beam current of 10 nA, 1–2 μm beam diameter). Samples were also examined by a LEO 1430 variable-pressure scanning electron microscope (SEM) instrument with a 3.5 nm spatial resolution operating at an accelerating voltage of 20 kV and using back-scattered electron (BSE) imaging and EDS analysis. Due to the fine-grained nature of the Ni- and Cu-rich mineral assemblages, a HRTEM study was performed using a Philips CM20 TEM-STEM instrument operating at 200 kV, $LaB_6$ filament, and equipped with an EDAX solid state detector. TEM grids, extracted from thin sections prepared with Canada balsam, were ion-thinned using a Gatan ion mill and then carbon coated.

## Weathering profile

The weathering profiles at the Aguablanca mine site formed *in situ* overlying the unaltered host gabbros, and they include several residual soil horizons. Soil profiles that form over ore-grade areas of the deposit are always more mature than those over barren areas. That is, they display a more evolved horizon sequence and concentrate the Ni- and Cu-bearing sheet silicates of interest (see mature profile in Fig. 2).

### Horizon sequence

Weathering profiles over ore-grade areas at Aguablanca are divided into four horizons named $A_h$, $B_{tg}$, C and R, based on their physicochemical properties. The superficial one is a reddish-brown horizon (less than 50 cm thick) that is topped by natural vegetation and accumulated organic material ($A_h$). It has a coarse texture with common gravels. In contrast, the following ~30 cm thick $B_{tg}$ greenish horizon has a fine-grained, homogeneous texture with a clay content twice that of the other profile horizons. It therefore shows strong changes in colour, texture and mineralogical composition downprofile. This horizon may be temporarily dampened towards its centre, but usually has a dry surface that shrinks and forms visible cracks favouring the formation of *slickensides*. Clay-coatings at both the macroscopic and microscopic scale denote some illuvial accumulation of clay minerals in this horizon ($B_t$). The mottled appearance of the soil aggregates also suggests the influence of temporary hydromorphic processes ($B_{tg}$). This horizon lies over the 1–2 m thick gabbroic lithologies (strongly weathered and little affected by pedogenetic processes, C horizon), and also fills open fractures. The unweathered hard gabbroic host rock lies below (bedrock, R horizon).

These soil profiles have a pH that varies between slightly acid near the surface [5.35–6.46] to neutral at depth [6.56–7.08]. The electrical conductivity [81.3–402.0 μS/cm], organic matter, and equivalent $CaCO_3$ are low (<4 wt%), and the highest values are always recorded upprofile. Water retention is also low, although it increases sharply in the B horizon (up to 35.03 %). The cation exchange capacity is moderate due to the regular presence of clays throughout the profile (13.26–56.28 $cmol_c$/kg), and the highest values are recorded in the B horizon. Saturation of the exchangeable complex is >50 %, with an average of 82.82 %.

### Soil geochemistry

The geochemistry of the soil profiles in ore-grade areas shows slight enrichments in $Al_2O_3$ (15.5 wt%, standard deviation ± 1.7) and $Fe_2O_3$ (18.8 wt% ± 2.6) towards the upper horizons (Fig. 2). In contrast, MgO, CaO and $Na_2O$ are leached in these levels. Silica is almost constant throughout the entire profile and $K_2O$, MnO, $TiO_2$, and $P_2O_5$ contents are low (<1 wt%).

The profiles show significant Ni, Cu and to a lesser extent Cr total contents (averages are 5850, 3780, and 1088 ppm, respectively) whereas S is always depleted (<3000 ppm), suggesting an intense loss of this element from the soil horizons. Also, a general impoverishment is observed in metals such as Co (average of 250 ppm), Zn (80 ppm), As, and Pb (<30 ppm). Despite this metal depletion, significant Ni and Cu enrichment occurs in the

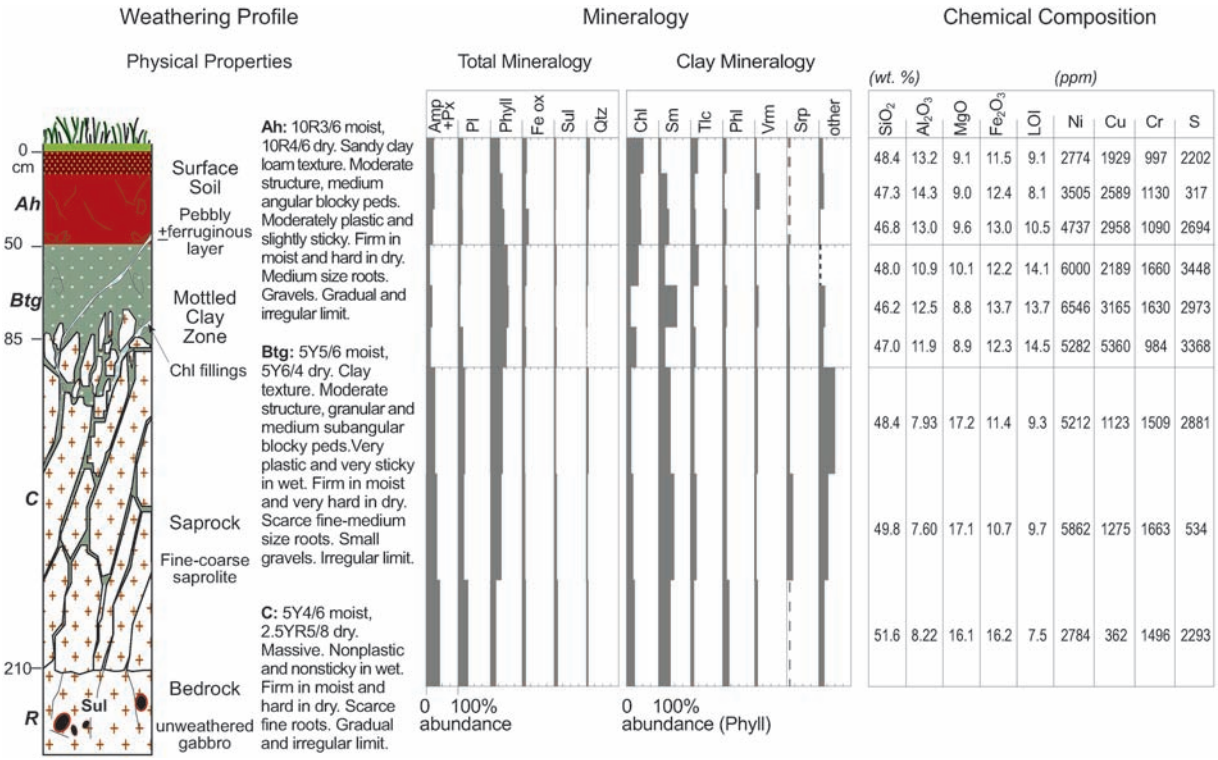


Fig. 2. Sketch of a weathering profile over irregular mineralization at the Aguablanca deposit.
Note: *Amp*, amphiboles; *Chl*, chlorite; *Fe ox*, Fe-oxides; *g*, mottled horizon reflecting temporary hydromorphic conditions; *h*, organic matter accumulation; *LOI*, lost on ignition; *other*, traces of detrital phases and mixed-layer clay minerals; *Phl*, phlogopite; *Phyll*, phyllosilicates; *Pl*, plagioclase; *Px*, pyroxenes; *Qtz*, quartz; *Sm*, smectite; *Srp*, serpentine; *Sul*, sulphides; *t*, illuvial accumulation of clay minerals; *Tlc*, Talc; *Vrm*, vermiculite.

clayey B horizons (average of 6934 ppm Ni and 5300 ppm Cu). The Ni and Cu concentrations in this horizon exceed those recorded in the A and C horizons by more than 2000 ppm. Within the B horizon, Ni, Cu, Co, and Cr show a good correlation with each other (Pearson correlation, $r = 0.7$), but they are poorly correlated with S ($r = -0.3$). In comparison, soil profiles over barren lithologies do not develop this B clay-rich horizon, and low Ni and Cu contents are only recorded in the uppermost A horizon (~1200 ppm).

## Mineralogical description of soil profiles

The mineralogy of the horizons within the Aguablanca soil profiles is complex, with recurrent primary igneous and hydrothermal relict minerals, but also several secondary phases able to retain metals. The distribution of the minerals throughout the soil profile is given in Fig. 2, and some SEM images of this mineralogy are shown in Fig. 3.

The residual mineralogy makes up the major fraction (up to 60 %) of the total mineralogy and mostly includes relicts of transformed silicates and minor sulphides (<15 % of the inherited fraction). The major silicate fraction comprises amphiboles (magnesiohornblende, actinolite, tremolite), pyroxenes (enstatite$_{56–77}$, diopside, augite), strongly altered plagioclase (an$_{3–58}$), Ti-rich magmatic and hydrothermal phlogopite ($X_{phl} = 0.67–0.77$), talc, chlorite, and rare quartz and pyrophyllite (Fig. 3a). Chlorite (clinochlore) and, to a lesser extent talc, are abundant through the entire profile, but especially towards the upper soil horizons.

Chlorite occurs firstly in aggregates within the bedrock as a product of an early hydrothermal stage (10–100 μm long, $Chl_1$). Chlorite that formed during later hydrothermal events occurs as large crystals filling fissures that crosscut the weathering profiles (up to 4 cm in length, $Chl_2$) (Fig. 3b, c). These chlorites may be transferred to the soil fraction, where they remain as detrital fragments (100 μm to ~1 cm long, $Chl_3$) (Fig. 3d). These two weathered chlorites ($Chl_{2–3}$) show rather similar XRD peak parameters (Fig. 4a, b), with mostly an *Ia* structure. In contrast, the unweathered chlorite in the bedrock ($Chl_1$) always has a regular *IIb* structure according to data reported by Brown & Bailey (1962), Bailey (1988a and b), and Weiss & Durovic (1983). The *Ia* polytype is characterized by the absence of the 2.45 Å peak (Fig. 4a), which is always strong for the *IIb* polytype. These *Ia* chlorites may show enhanced 002 and 004 reflections towards upper horizons, probably because of the common serpentine intergrowth, and reflect the presence of some less stable layers within the sheets, as they diminish in basal intensities after heat treatments.

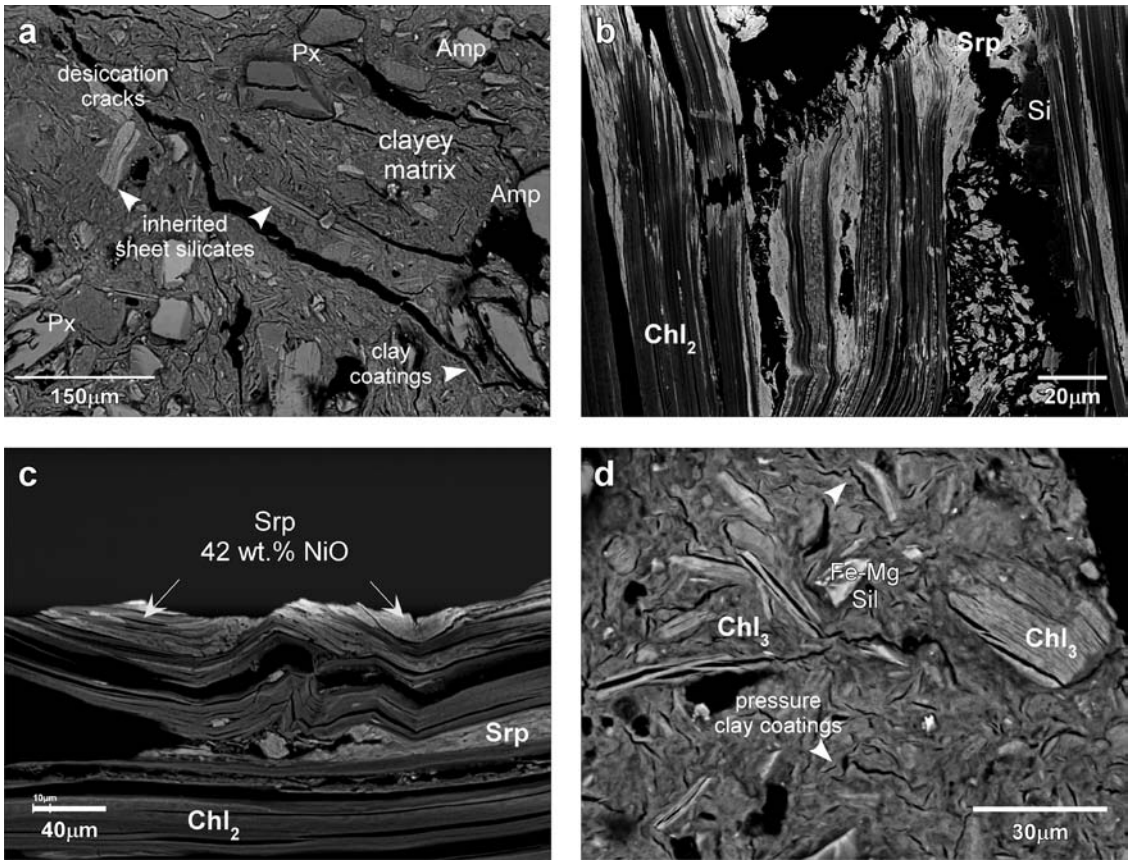


Fig. 3. SEM images of the soil samples at the Aguablanca mine site. (a) The B horizon, with a large clayey matrix and significant, poorly reworked, inherited silicates; (b, c) chlorite filling fissures throughout the weathering profile ($Chl_2$), with serpentine at the crystal edges and filling textural defects; (d) concentration of chlorite sheets within the soil horizons ($Chl_3$).
Note: *Amp*, amphiboles; *Chl*, chlorite; *Px*, pyroxenes; *Si*, silica; *Sil*, silicates; *Srp*, serpentine.

Serpentine occurs as microcrystalline aggregates of lizardite intergrown with chlorite crystals throughout the soil profile ($Chl_{2-3}$). The small size of the aggregates has prevented any characterization of serpentine by optical microscopy or EMP. However, SEM images reveal that serpentine mostly occurs at the edges of chlorite crystals, filling textural defects, and as coatings in cavity walls along the laths of chlorite. In detail, the aggregates of serpentine may host small fragments of chlorite, and colloidal silica is rarely observed on the outside of the aggregates (Fig. 3b, c).

Deconvolution of the diffraction patterns of altered chlorites ($Chl_{2-3}$) revealed two peaks contributing to the bands observed at 12.13–12.59 °2θ and 24.3–25.8 °2θ. In the first band, a broad peak is centred near 7.138 Å and corresponds to chlorite, whereas the other smaller peak that occurs between 7.168 and 7.1940 Å should be lizardite. In the second region, the XRD pattern of serpentine yields a reflection at about 3.59 Å (*peak 1*, Fig. 4a) whereas chlorite is fixed at 3.57 Å (*peak 2*, Fig. 4a). This close juxtaposition of the two components produces spacings seemingly closer than the real ones. The weak reflection at ~4.60 Å in the XRD patterns (observed intensity of ~30–40 %) resembles the non-basal (020) reflection of Ni-lizardite. This reflection has been described as weak for nepouite (Ni-lizardite end-member), prominent for nickeliferous lizardite, and sharp for Mg-lizardite at smaller spacings of about 4.55 Å (Brindley & Wan, 1975).

On the basis of the weak reflections, the 1.50 Å peak also suggests a Ni-lizardite/nepouite since Ni-chrysotile/pecoraite displays a strong, solitary reflection at ~1.53 Å (Nickel *et al.*, 1994). As concerns the layer stacking sequence, the strong 2.387 Å reflection and the invariable absence of the 2.49 Å peak are probably indicative of group A (~$2M_1$ polytype). The most intense reflection at 2.326 Å of group B and the 1.945 Å peak of groups B and D are also absent. Group A is characteristic of 1:1 layer silicates with relatively low structural stability in nature (Bailey, 1969).

Apart from serpentine, the secondary mineralogy also includes scarce nodules of Fe-(Ni-Cu) oxides near the soil surface and mostly soil clay minerals that are particularly abundant in the B horizon (up to 56 % volume). This clay fraction mainly includes smectite, vermiculite, and mixed-layer minerals. Smectite is profuse throughout the profiles except at the soil surface, where conditions

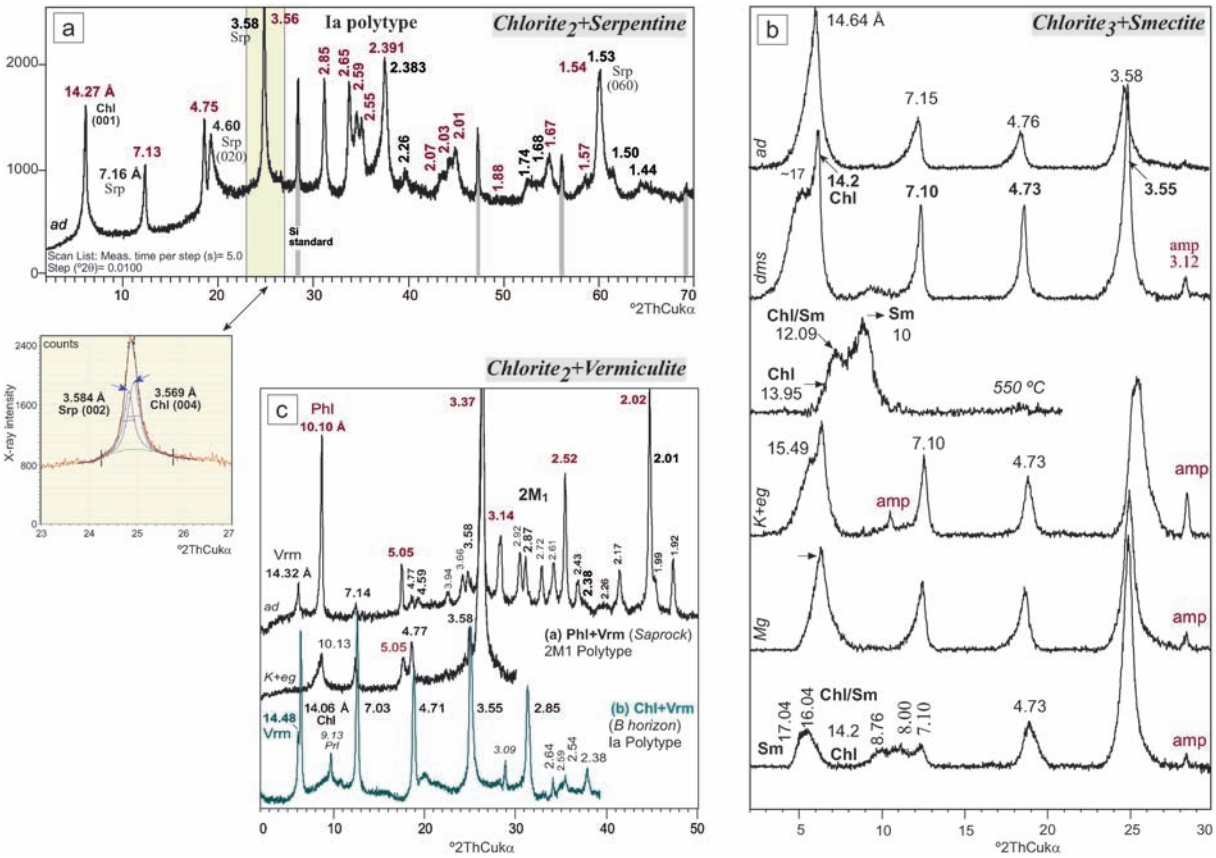


Fig. 4. XRD patterns for the main Ni-Cu-bearing sheet silicates at the Aguablanca deposit. (a) Chlorite in fissures ($Chl_2$) intergrown with serpentine. Note diagnostic reflections for the *Ia* polytype. The arrow points to the fit of the 24.3–25.8 °2θ serpentine band. *1* (serpentine) and *2* (chlorite) are the individual peaks determined by the fitting routine. Solid black line represents the composite profile formed by peaks *1* and *2*; (b) chlorite ($Chl_3$) and smectite within the weathered horizons; (c) vermiculite associated with phlogopite and chlorite within the weathered horizons. Note: *ad*, air dried; *Amp*, amphiboles; *Chl*, chlorite; *Chl/Sm*, mixed-layer chlorite/smectite; *dms*, dimethyl sulfoxide; *eg*, ethylene-glycol; *En*, enstatite; *g*, glycerol solvation; *K*, $K^+$saturation; *Mg*, $Mg^{2+}$saturation; *Phl*, phlogopite; *Prl*, pyrophyllite; *Qtz*, quartz; *Sil*, silicates; *Sm*, smectite; *Tlc*, talc; *Vrm*, vermiculite.

turn slightly acid. It is often associated with chlorite within the soil horizons and fissures cross-cutting the profile ($Chl_{2-3}$). Mainly beidellite, nontronite, and saponite are identified in the clay fraction based on (060) reflections and the Greene-Kelly test (Greene-Kelly 1952, 1953; Byström-Brusewitz, 1975). Second-order reflections at about $d$ =12 Å (heat treatment) and 16 Å (Mg saturation-glycerol solvation) reflect regular Chl/Sm interstratified mixed-layer minerals (corrensite) (Fig. 4b), but superstructures at ~31 Å in air-dried samples rarely occur. Vermiculite is a much less abundant mineral compared to smectite. It is commonly associated with chlorite and phlogopite (Fig. 4c), and can be regularly interstratified with both components. It has a common first-order reflection at ~14.4 Å, low full width at half maximum (FWHM parameter) of <0.1 °2θ, and (060) spacing of about ~1.541 Å that indicates a trioctahedral character. $K^+$-saturation and heat treatments always collapse vermiculite to 10.1 Å, and it is therefore not a hydroxy-interlayered mineral typical of moderately oxidized soil horizons (*e.g.*, Meunier, 2007).

## Base-metal contents. Mineral chemistry of the host phases

Bulk Ni and Cu contents recorded for the main mineralogy using the EMP (and SEM-EDS for serpentine) are plotted in Fig. 5, and some representative analyses are given in Table 1. These results show that the residual mineralogy retains little Ni or Cu, except for chlorite. NiO and CuO contents recorded in amphiboles, pyroxenes, feldspars, phlogopite and talc range from zero to 0.3 wt%, with the maximum values recorded in phlogopite and talc. In contrast, clinochlore within the soil horizons ($Chl_{2-3}$) shows up to 12.5 wt% NiO and 9 wt% CuO; although these contents could be enhanced due to the usual intergrowth of serpentine.

The secondary minerals within the soil horizons all host variable Ni and Cu, but serpentine shows the highest Ni contents recorded (up to 44 wt% NiO) and occasional Cu (average of 3.7 wt% CuO). Smectite-, vermiculite- and corrensite-like minerals seem to be less effective Ni and Cu scavengers and retain up to 3.9 wt% NiO and 2.9 wt%

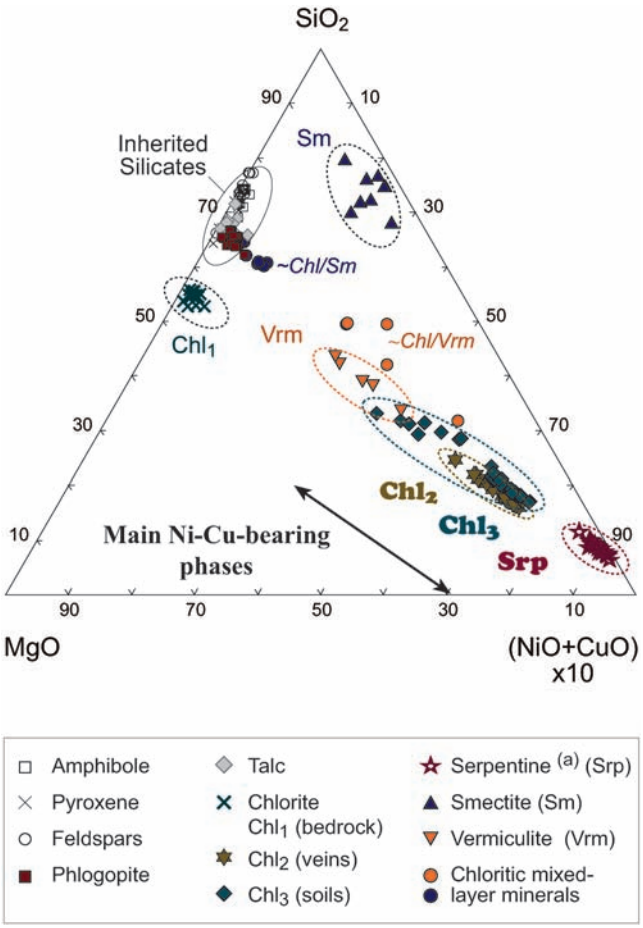


Fig. 5. Bulk Ni and Cu contents in the main minerals of the Aguablanca weathering profiles (A, B, and C horizons), as determined by EMP and EDS analyses[a]. Analyses of chlorite in the underlying fresh bedrock (*Chl$_1$*) are also included for comparison.
Note: [a]SEM-EDS analyses of serpentine.

CuO. Analyses of nodules of Fe-oxides dispersed throughout the upper soil horizons revealed lower metal contents compared to the soil clay mineralogy ($\leq$0.3 wt% NiO and CuO). The analogous clay mineralogy in barren soil profiles within the *Contact Gabbro* showed negligible Ni and Cu contents in its composition; rarely, up to 0.5 wt% NiO and 0.1 wt% CuO were recorded.

These bulk analyses indicate that weathered chlorite ($Chl_{2-3}$), together with the closely associated Ni-lizardite, are the main Ni-Cu-bearing phases in the ore-grade soil profiles of the Aguablanca deposit. However, Ni seems to be largely retained by serpentine whereas Cu is preferentially retained by chlorite, as detailed next.

***Chlorite*** in the fresh rock ($Chl_1$) is an ordinary clinochlore with moderate Fe substitution (r Fe/Mg = $-0.91$). Tetrahedral substitution is constant and Si is well correlated with total Al (r Si/Al = $-0.97$, r $Al^{VI}/Al^{IV} = 0.82$). The sum of octahedral cations ranges from 5.75 to 5.98 ($\pm$0.05). However, this composition changes notably in the weathered parts of the profiles. Chlorite both in fissures ($Chl_2$) and within the horizons ($Chl_3$) reflects mixed compositions, with very high Si contents (average of 3.3 afu $\pm$ 0.1; 30.65 wt% $SiO_2$ $\pm$ 1.59) and minor $K^+$, $Na^+$, and $Ca^{2+}$ impurities (average of 0.37 wt% oxides, 0.04 total afu). Silica is well correlated with total Al, and tetrahedral substitution is rather constant. Nickel and Cu are abundant in these chlorites, with higher Cu contents in $Chl_2$ at open fissures (up to 0.72 afu Cu, 0.37 afu Ni), and higher Ni contents in $Chl_3$ within the horizons (up to 1.05 afu Ni, 0.54 afu Cu) (see Table 1). In both cases, the Fe-Mg inverse tendency is absent, and Mg is inversely correlated with Ni and Cu (r Mg/Ni+Cu= $-0.96$ in $Chl_2$; $r = -0.55$ in $Chl_3$). Total octahedral cations range from 5.6 to 6.01 afu.

***Serpentine*** also has a mixed composition as determined by EDS analyses (Table 1). Average $SiO_2$ content is 37.06 wt% (1.9 afu $\pm$ 0.06) and minor impurities of $K^+$ and $Ca^{2+}$ are detected (0.02 total afu). Octahedral cations are mainly Ni (up to 1.95 afu $\pm$ 0.29) and minor Cu ($\leq$0.24 afu $\pm$ 0.08) (see Table 1). Nickel is inversely correlated with Mg and $Al^{VI}$ ($r = -0.8$), whereas Cu is poorly correlated with these elements. Tetrahedral substitution is variable and total octahedral cations sum 2.91 afu on average ($\pm$0.05).

Base-metals recorded on ***smectite, vermiculite, and mixed-layer minerals*** (Table 1) are always assumed as octahedral cations. The cation-exchange procedure carried out on clay-rich samples showed that Fe, Ni, and Cu

Table 1. Representative EMP and EDS[(a)] analyses of the main Ni- and Cu-bearing sheet silicates in the Aguablanca soil profiles. Summary of the NiO and CuO contents of each phase (wt. %) are given below.

| | Chlorite | | | | | | | | | | | | Serpentine[a] | | | |
|---|---|---|---|---|---|---|---|---|---|---|---|---|---|---|---|---|
| | $Chl_1$ (Rock) | | | | $Chl_2$ (Vein) | | | | $Chl_3$ (Horizon) | | | | | | | |
| (wt%) | 1 | 2 | 3 | 4 | 5 | 6 | 7 | 8 | 9 | 10 | 11 | 12 | 1 | 2 | 3 | 4 |
| $SiO_2$ | 28.59 | 28.42 | 28.73 | 28.38 | 28.66 | 29.92 | 30.19 | 30.84 | 29.45 | 29.25 | 29.48 | 28.50 | 35.38 | 37.99 | 36.32 | 37.42 |
| $TiO_2$ | 0.02 | 0.03 | – | 0.04 | 0.31 | 0.30 | 0.34 | 0.30 | – | – | – | – | 0.24 | – | 0.23 | 0.51 |
| $Al_2O_3$ | 19.85 | 19.40 | 19.83 | 19.70 | 16.79 | 17.61 | 17.14 | 17.89 | 11.08 | 12.02 | 10.59 | 10.56 | 10.31 | 3.54 | 6.65 | 6.59 |
| $Cr_2O_3$ | 0.02 | 0.04 | 0.05 | – | 0.01 | – | – | 0.02 | – | – | – | – | – | – | – | – |
| FeO | 16.08 | 16.29 | 16.01 | 17.28 | 4.66 | 4.77 | 5.01 | 5.04 | 16.22 | 16.05 | 16.82 | 16.72 | 3.58 | 5.73 | 3.36 | 11.57 |
| MnO | 0.26 | 0.29 | 0.28 | 0.30 | 0.23 | 0.25 | 0.28 | 0.25 | 0.29 | 0.12 | 0.17 | 0.04 | – | – | – | – |
| MgO | 22.43 | 22.55 | 22.43 | 21.83 | 18.97 | 19.86 | 20.37 | 20.98 | 16.43 | 16.22 | 16.53 | 16.08 | 13.59 | 7.74 | 10.01 | 9.46 |
| NiO | 0.08 | 0.12 | 0.16 | 0.11 | 4.29 | 4.29 | 3.83 | 4.21 | 9.93 | 10.24 | 9.84 | 9.57 | 30.81 | 43.89 | 37.83 | 29.25 |
| CuO | 0.04 | – | 0.01 | – | 8.87 | 9.06 | 6.71 | 8.15 | 1.01 | 0.70 | 0.40 | 0.34 | 5.68 | 0.89 | 5.06 | 4.79 |
| CoO | – | – | – | – | – | – | – | – | – | – | – | – | – | – | – | 0.42 |
| CaO | 0.06 | 0.03 | 0.06 | 0.03 | 0.30 | 0.29 | 0.39 | 0.32 | 0.18 | 0.12 | 0.11 | 0.12 | 0.25 | 0.21 | 0.38 | – |
| $Na_2O$ | – | – | 0.04 | 0.01 | – | 0.01 | 0.04 | 0.02 | – | 0.03 | – | 0.04 | – | – | – | – |
| $K_2O$ | – | 0.02 | 0.03 | 0.03 | 0.08 | 0.08 | 0.10 | 0.10 | 0.03 | 0.04 | 0.03 | 0.05 | 0.16 | – | 0.16 | – |
| Total | 87.43 | 87.21 | 87.63 | 87.71 | 83.15 | 86.45 | 84.39 | 88.13 | 84.61 | 84.79 | 83.96 | 82.00 | 100 | 100 | 100 | 100 |

Smectite-, Vermiculite-, and Corrensite-like minerals

| | *Sp* | *Bd* | | *Nnt* | | *Vermiculite* | | | | *Corrensite* | | | |
|---|---|---|---|---|---|---|---|---|---|---|---|---|---|
| (wt.%) | 1 | 2 | 3 | 4 | 5 | 1 | 2 | 3 | 4 | 1 | 2 | 3 | 4 |
| $SiO_2$ | 41.73 | 42.40 | 42.49 | 42.60 | 44.93 | 37.19 | 35.89 | 37.07 | 35.02 | 35.62 | 38.54 | 35.96 | 41.46 |
| $TiO_2$ | 0.50 | – | – | – | – | 0.43 | 0.41 | 0.43 | 0.37 | – | 4.87 | – | – |
| $Al_2O_3$ | 15.14 | 18.09 | 17.38 | 5.05 | 12.94 | 17.96 | 17.95 | 17.99 | 17.09 | 19.88 | 13.14 | 14.42 | 12.80 |
| $Cr_2O_3$ | 0.20 | – | – | – | – | – | 0.01 | 0.00 | 0.02 | – | 0.31 | – | – |
| $Fe_2O_3$ | 8.44 | 12.52 | 13.12 | 24.43 | 14.29 | 5.07 | 5.25 | 5.33 | 5.42 | – | – | – | – |
| FeO | 0.00 | 0.00 | 0.00 | 0.00 | 0.00 | 0.00 | 0.00 | 0.00 | 0.00 | 7.57 | 10.75 | 15.83 | 12.47 |
| MnO | 0.05 | 0.06 | 0.05 | – | 0.03 | 0.26 | 0.20 | 0.31 | 0.26 | 0.08 | 0.06 | 0.25 | 0.14 |
| MgO | 22.88 | 2.87 | 1.67 | 1.64 | 3.95 | 21.93 | 21.85 | 22.70 | 21.43 | 15.76 | 16.29 | 10.85 | 17.88 |
| NiO | 0.14 | 1.22 | 0.90 | 0.79 | 0.89 | 2.01 | 1.97 | 1.75 | 1.69 | 2.95 | 1.03 | 2.05 | 2.07 |
| CuO | 0.02 | 0.52 | 0.40 | 0.36 | 0.47 | 1.75 | 2.87 | 1.02 | 1.62 | 0.41 | 1.25 | 0.54 | 0.38 |
| CoO | – | – | – | – | – | – | – | – | – | – | – | – | – |
| CaO | 0.18 | 0.60 | – | 1.60 | 0.36 | 0.41 | 0.34 | 0.47 | 0.96 | 0.39 | 0.76 | 0.57 | 0.58 |
| $Na_2O$ | – | 0.14 | 0.12 | 0.27 | 0.11 | – | 0.01 | 0.01 | 0.06 | 0.09 | 0.13 | 0.05 | 0.08 |
| $K_2O$ | 0.02 | 0.50 | – | 0.14 | 0.32 | 0.04 | 0.04 | 0.08 | 0.47 | – | 0.42 | 0.09 | 0.11 |
| Total | 89.32 | 78.91 | 76.14 | 76.90 | 78.30 | 87.04 | 86.79 | 87.15 | 84.41 | 82.75 | 87.55 | 80.61 | 87.96 |

| | | NiO wt. % | | | | CuO wt. % | | | |
|---|---|---|---|---|---|---|---|---|---|
| | *n* | Min | Max | Mean | StDv | Min | Max | Mean | StDv |
| $Chl_1$ | *15* | 0.05 | 0.16 | 0.11 | 0.03 | 0.00 | 0.16 | 0.03 | 0.04 |
| $Chl_2$ | *13* | 3.39 | 4.30 | 3.99 | 0.32 | 4.60 | 9.06 | 7.16 | 1.54 |
| $Chl_3$ | *46* | 2.33 | 12.47 | 8.04 | 2.70 | 0.24 | 6.88 | 1.89 | 1.74 |
| Srp | *9* | 28.15 | 44.07 | 34.82 | 6.10 | 0.86 | 5.83 | 3.71 | 2.14 |
| Sm | *11* | 0.04 | 1.22 | 0.73 | 0.36 | 0.02 | 0.52 | 0.31 | 0.16 |
| Vrm | *5* | 1.63 | 2.01 | 1.81 | 0.17 | 0.93 | 2.87 | 1.64 | 0.78 |
| Corr | *11* | 0.20 | 3.92 | 2.06 | 1.25 | 0.02 | 2.16 | 1.09 | 0.65 |

Note: *afu* atoms per formula unit, *Bd* beidellite, *Chl* chlorite, *Corr* corrensite-like minerals, *Max* maximum, *Min* minimum, *n* number of analyses, *Nnt* nontronite, *Sm* smectite, *Sp* saponite, *Srp* serpentine, *StDv* standard deviation, *Vrm* vermiculite, – not detected; [(a)]SEM-EDS analyses of serpentine.

contents were negligible in the exchangeable fraction (3.8, 10.4, and 17.8 ppm, respectively). Conversely, moderate contents in Mg and Ca (from 1450 to 3000 ppm), and lesser amounts of Na and K (<100 ppm), were recorded in this fraction. Thus, the Mg excess recorded in the smectite and vermiculite analyses can be related to the interlayer spaces of their structures (without exceeding the maximum theoretical charge per formula unit in each case; as per

Bailey, 1980). Several smectite species were detected, ranging between the di- and trioctahedral varieties, all with low Ni and Cu contents (≤0.15 afu). Similar Ni and Cu contents are recorded in vermiculite (≤0.22 afu) and these contents increase slightly in corrensite (≤0.9 afu) (see Table 1).

## TEM study of the Ni-Cu-bearing sheet silicates

### TEM observations

***Chlorite*** occurs in well-defined 14.0–14.2 Å packets (Fig. 6a), although areas with intergrown smectite are very common. These areas show irregular alternations of 14 Å and thin 10-10.2 Å layers (Fig. 6b), and some mixed 24–24.2 Å layers may occur (Fig. 6c). Saponite, together with corrensite, occurs largely interleaved with chlorite ($Chl_{2-3}$), whereas dioctahedral smectites are preferentially associated with other inherited silicates like amphibole or talc throughout the soil profiles. Chlorite is also progressively transformed to vermiculite, increasing basal spacings up to 14.5–15 Å (Fig. 6d).

The specimens of chlorite examined ($Chl_{2-3}$) all show small particles of native Cu metal that range from 5 to 150 nm in width and are up to 1200 nm in length (Fig. 6e). These Cu particles are strongly associated with the expanded domains of chlorite, where a 10 or 12 Å-smectite commonly occurs (Fig. 6f). They are mainly elongate inclusions with polygonal morphologies that often show complex intergrowths and may be twinned (Fig. 6g), as frequently occurs across the {111} planes in metals like Cu (*e.g.*, Davis, 2001). Convergent beam electron diffraction patterns from several Cu particles, together with the EDS analyses (Fig. 6h, i), are consistent with the identification of these inclusions as native copper. The particles show a face-centred cubic structure and up to 92.8 wt% Cu in the composition. Minor impurities of O, Mg, Fe, Si, or Al were occasionally recorded (<2.6 wt%) and these may belong to the host chlorite.

Copper particles are also widespread in smectite laths. They are occasionally observed in phlogopite within the soil horizons, usually enclosed in altered domains where vermiculite or ~24.45 Å layers develop. Copper particles are scarce in talc and were not observed in serpentine.

***Serpentine***. TEM images in regular domains of serpentine reveal large areas of well-defined 7 Å spaced lattice-fringes with flat layering (Fig. 7a). Boundaries between serpentine and chlorite may show 21.2 Å layers suggesting some interstratification between the two components (Fig. 7b), but more often these junctions show regular intergrowths of thin 14 Å packets and well-developed 7 Å layers (Fig. 7c). Serpentine seems to crystallize in monomineralic stacks, although selected area electron-diffraction (SAED) patterns occasionally show some smectite contamination. However, well-defined 10 Å fringes were not observed.

Highly altered laths of serpentine show small (3–30 nm) sub-rounded to elongate Ni-(Fe ± Cu)-rich particles mainly at their edges. These tiny particles may be isolated or form clusters irregularly distributed along the (001) layers of serpentine (Fig. 7d, e). EDS analyses of the largest particles reveal that these are mainly composed of Ni (between 79 and 97 wt%), although small amounts of Fe and less Cu (≤11 wt%) are also detected (Fig. 7f). Minor impurities of O, Mg, and Si (≤2 wt%) are often recorded. Nevertheless, the small size of these particles precludes determining whether these are true stoichiometric phases similar to any metallic or intermetallic alloys (*e.g.*, awaruite, $Ni_3Fe$) or whether they are clusters of intermetallic amorphous compounds.

***Smectite, vermiculite and corrensite***. Smectite was mainly observed in two different assemblages: (i) Saponite typically occurs interleaved with chlorite ($Chl_{2-3}$) through the soil horizons, and they may form corrensite-like minerals. This saponite usually hosts the Cu particles recognized in chlorite crystals (see Fig. 6); (ii) Dioctahedral smectites, mainly beidellite and minor nontronite, occur widespread throughout the soil profile. They can be associated with chlorite but they are observed mainly as an alteration product of other inherited silicates downprofile. Lattice-fringe images evidence incipient vermiculite in thin 14.5 Å packets intergrown with chlorite (see Fig. 6), although vermiculite associated with phlogopite is more frequent. It grows at the edges of the phlogopite crystals but is also associated with the expanded domains, where Cu particles may appear, and superstructures may form at ~24.45 Å.

### AEM data

The AEM analyses were performed on regular, uncontaminated layers of the Ni-Cu-bearing sheet silicates and avoiding those domains where Cu or Ni particles occur (see Table 2 for representative analyses).

***Chlorite***. AEM analysis of $Chl_2$ within fractures shows average Ni contents similar to those obtained using the EMP, whereas Cu contents decrease significantly (from 0.6 to 0.16 afu on average). Both Ni and Cu are inversely correlated with Mg (r Mg/Ni+Cu= −0.75). The sum of octahedral cations ranges from 5.61 to 6.02, and some $Ca^{2+}$ and $K^+$ are detected. Tetrahedral substitution is variable and high average Si contents are recorded (3.26 afu ± 0.13). Successful AEM analyses of $Chl_3$ dispersed in the soil horizons were not possible since this chlorite always has a strong mixed composition.

***Serpentine***. AEM analyses of the ordered 7 Å spaced lizardite yield high Ni contents (average of 1.35 afu ± 0.33) but rare Cu in its composition. Nickel is inversely correlated with Mg ($r = -0.78$) and $Al^{VI}$ ($r = -0.83$), but is poorly correlated with other chemical parameters. Tetrahedral substitution is variable and the sum of octahedral cations is 2.85 on average (±0.09). This serpentine is therefore classified as an intermediate phase between the Mg and Ni end-members of the

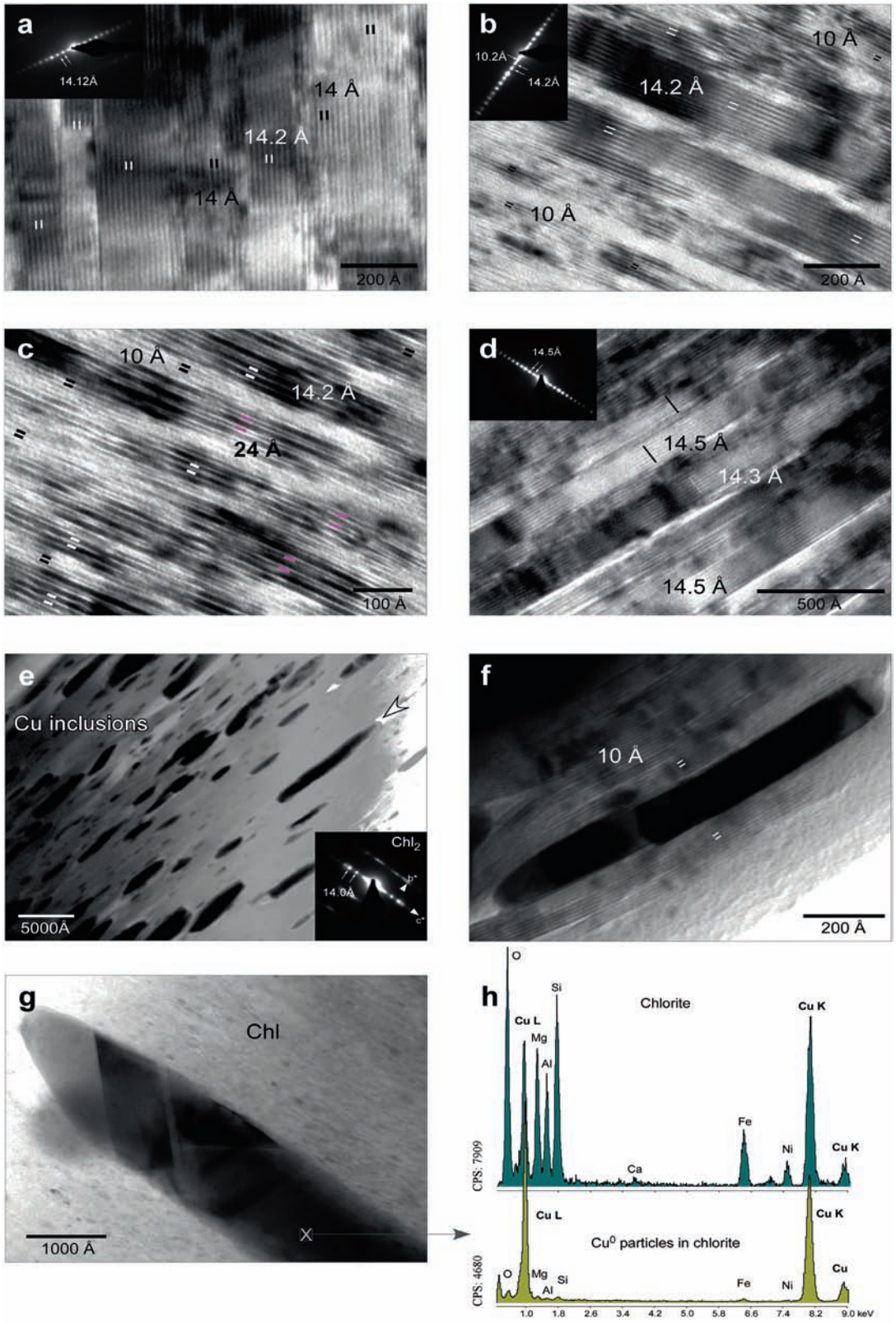


Fig. 6. TEM images of chlorite ($Chl_{2-3}$) in the soil profiles of the Aguablanca deposit. (a) Lattice-fringe image showing regular layers of chlorite; (b) intergrowth of chlorite and smectite; (c) layers of corrensite (10+14.2 Å) in chlorite; (d) vermiculitization of chlorite; (e) textural image showing profuse Cu particles within expanded domains in chlorite; (f) intergrowth of several Cu particles within a deformed smectite lamella; (g) an example of twinning in a Cu particle; (h) EDS spectrum of the regular domains of chlorite (top) and of a Cu particle (bottom); (i) convergent beam electron diffraction patterns from a Cu particle showing the [101], [110], [111] and [112] zone axis of metallic Cu.
Note: *Chl*, chlorite; *CPS*, counts per second.

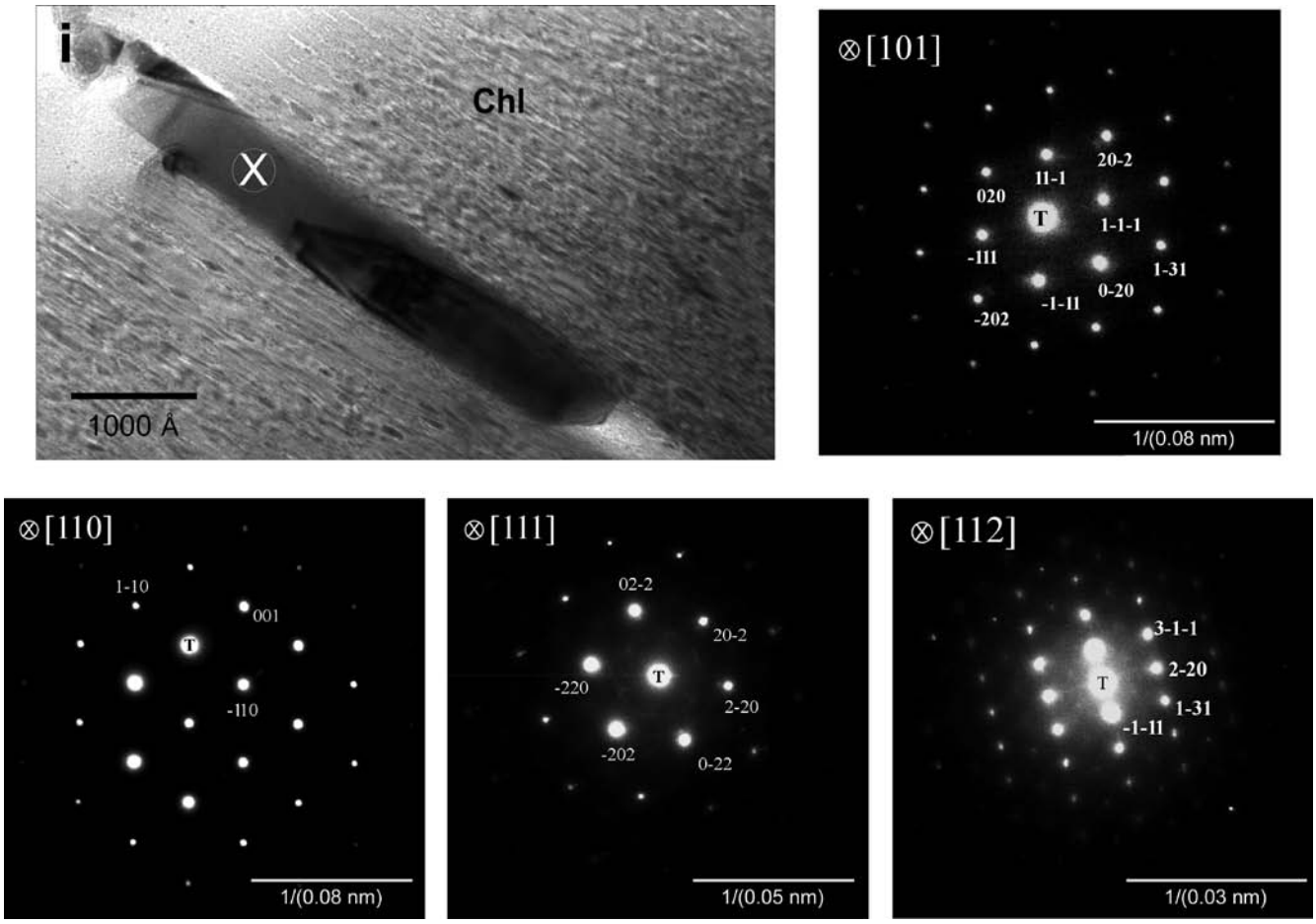


Fig. 6. Continued.

lizardite-nepouite series (*e.g.*, Brindley & Wan, 1975; Maksimović, 1975; Manceau & Calas, 1985, 1986), although it shows a greater tendency towards the nepouite composition (Ni > Mg and Ni > 1.5 afu). Based on the Ni content, it falls into the *garnierite* field delimited by Gleeson *et al.* (2003) (Fig. 8).

Representative AEM analyses carried out on ***smectite and corrensite*** throughout the soil horizons reveal a recurrent mixed composition for these phases, with variable structural Ni contents, but rare Cu. Corrensite retains similar or even higher Ni contents than those recorded in pure chlorite layers (up to 1.6 afu $Ni^{2+}$). AEM data also reveal several smectite species, with saponite retaining higher contents of base-metals (up to 0.23 afu $Ni^{2+}$ and 0.27 afu $Cu^{2+}$) compared to beidellite and nontronite (<0.1 afu $Ni^{2+}$ and $Cu^{2+}$). AEM analyses of vermiculite were not successful, although it showed the same trend, with moderate Ni but little Cu in its composition. In short, AEM analyses reflect less Ni, and particularly less Cu, structurally bound to the sheet silicates compared to the bulk results obtained using the EMP.

## Discussion

Anomalous Ni and Cu associated with sheet silicates at the Aguablanca deposit seem to be restricted to the ore-grade weathered domain of the *Gabbronorite Unit*. This is primarily evidenced by the B soil horizon and particularly in areas far from the orebodies, where sheet silicates are highly concentrated and coincide with a clear enhancement of the bulk Ni and Cu contents recorded throughout the profiles. Furthermore, Ni and Cu are preferentially concentrated in weathered sheet silicates that are not associated with relic sulphides in the soil matrix. Finally, analogous sheet silicates in the underlying host rocks or within barren profiles at the deposit host negligible Ni and Cu contents. Consequently, it is likely that Ni and Cu were introduced into the sheet silicates after the dissolution of sulphides in ore-grade areas of the deposit, probably from $Ni^{2+}$- and $Cu^{2+}$-rich weathering solutions.

Within the soil profiles examined at Aguablanca there are several types of inherited and newly formed sheet silicates that retain variable Ni and Cu. These phases reveal

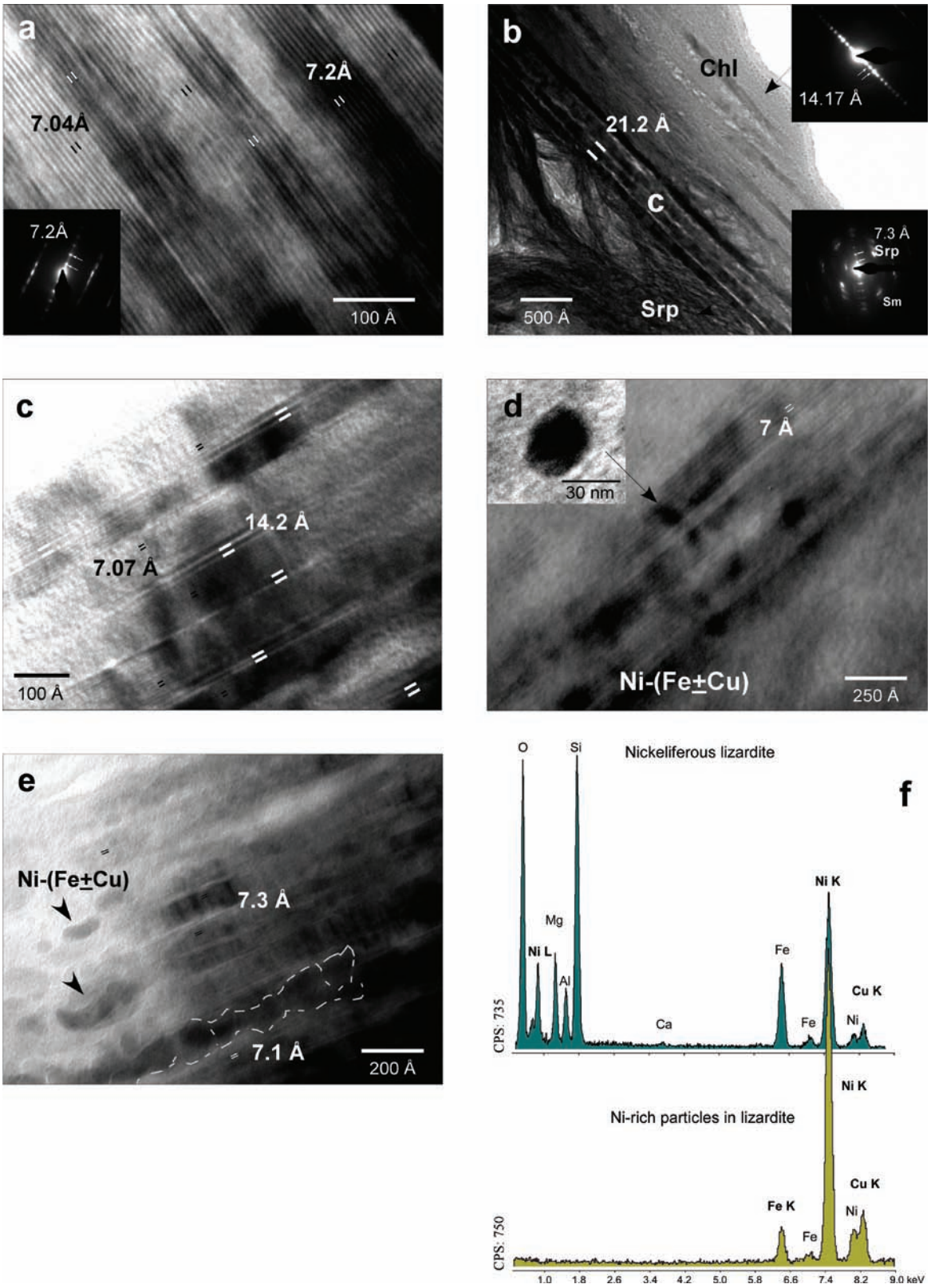


Fig. 7. TEM images of nepouite-like minerals at the Aguablanca deposit. (a) Lattice-fringe image showing regular layers of lizardite; (b) Chl/Srp (14+7 Å) at the junction of chlorite and serpentine; (c) common intergrowth of chlorite and serpentine at these junctions; (d, e) Ni-(±Fe-Cu) particles along altered laths of serpentine; (f) EDS spectrum of the regular domains of serpentine (top) and of a Ni-(±Fe-Cu) particle (bottom).

Note: *Chl*, chlorite; *CPS*, count per second; *Sm*, Smectite; *Srp*, serpentine.

Table 2. Normalized AEM analyses performed on regular layers of chlorite, serpentine, smectite and on corrensite from the Aguablanca soil profiles.

| | Chlorite$_2$ (Vein) | | | | | | | | | | Serpentine | | | | | | | | | | | Smectite, Corrensite | | | | | | | | | | |
|---|---|---|---|---|---|---|---|---|---|---|---|---|---|---|---|---|---|---|---|---|---|---|---|---|---|---|---|---|---|---|---|---|
| | | | | | | | | | | | | | | | | | | | | | | *Sp* | | *Bd* | | *Nnt* | Corrensite | | | | | |
| *(afu)* | 1 | 2 | 3 | 4 | 5 | 6 | 7 | 8 | 9 | 10 | 1 | 2 | 3 | 4 | 5 | 6 | 7 | 8 | 9 | 10 | 11 | 1 | 2 | 3 | 4 | 5 | 6 | 7 | 8 | 9 | 10 | 11 |
| Si | 3.21 | 3.19 | 3.01 | 3.29 | 3.14 | 3.29 | 3.32 | 3.36 | 3.33 | 3.44 | 1.82 | 1.80 | 1.98 | 2.03 | 1.97 | 1.98 | 1.92 | 1.92 | 1.94 | 1.98 | 1.86 | 2.95 | 3.03 | 3.55 | 3.50 | 3.43 | 6.28 | 6.29 | 6.36 | 6.55 | 6.51 | 7.33 |
| $Al^{IV}$ | 0.79 | 0.81 | 0.99 | 0.71 | 0.86 | 0.71 | 0.68 | 0.64 | 0.67 | 0.56 | 0.18 | 0.20 | 0.02 | 0.00 | 0.03 | 0.02 | 0.09 | 0.08 | 0.06 | 0.02 | 0.14 | 1.05 | 0.97 | 0.45 | 0.50 | 0.57 | 1.72 | 1.71 | 1.64 | 1.45 | 1.49 | 0.67 |
| Ti | 0.07 | 0.02 | – | – | – | 0.07 | – | 0.02 | – | 0.02 | – | – | 0.01 | – | – | – | 0.03 | – | – | – | – | 0.02 | 0.02 | 0.02 | 0.02 | – | 0.17 | 1.16 | 0.83 | 0.66 | 0.54 | – |
| $Al^{VI}$ | 1.17 | 1.32 | 1.09 | 1.10 | 0.82 | 0.86 | 1.39 | 1.30 | 1.29 | 1.21 | 0.09 | 0.11 | 0.28 | 0.27 | 0.34 | 0.15 | 0.46 | 0.26 | 0.36 | 0.45 | 0.58 | 0.49 | 0.48 | 1.05 | 0.98 | 0.31 | 1.32 | 0.60 | 0.93 | 1.44 | 1.42 | 1.97 |
| Cr | – | – | – | – | – | – | – | – | – | – | – | – | – | – | – | – | – | – | – | – | – | – | – | – | – | – | – | 0.08 | 0.08 | 0.04 | 0.04 | – |
| Fe | 0.38 | 0.62 | 0.88 | 0.95 | 1.80 | 1.45 | 0.38 | 0.43 | 0.54 | 1.16 | 0.54 | 0.68 | 0.53 | 0.18 | 0.63 | 0.36 | 0.40 | 0.34 | 0.18 | 0.10 | 0.11 | 0.27 | 0.27 | 0.83 | 0.92 | 1.59 | 1.60 | 3.10 | 3.64 | 1.77 | 2.28 | 1.57 |
| Mn | – | 0.02 | – | 0.07 | – | 0.05 | – | – | 0.02 | 0.09 | – | – | – | – | – | – | 0.01 | – | – | – | – | – | – | – | – | – | – | – | – | – | – | 0.12 |
| Mg | 3.82 | 3.52 | 3.66 | 3.45 | 3.00 | 2.41 | 3.47 | 3.19 | 2.79 | 2.74 | 0.68 | 0.73 | 0.66 | 0.61 | 0.69 | 0.66 | 0.97 | 0.73 | 0.98 | 0.91 | 1.18 | 2.10 | 2.02 | 0.06 | 0.05 | 0.10 | 4.22 | 2.48 | 2.27 | 4.08 | 3.73 | 3.58 |
| Ni | 0.26 | 0.17 | 0.14 | 0.14 | 0.26 | 0.48 | 0.40 | 0.31 | 0.43 | 0.24 | 1.70 | 1.48 | 1.35 | 1.72 | 1.16 | 1.75 | 0.79 | 1.57 | 1.32 | 1.30 | 0.89 | 0.13 | 0.20 | 0.03 | 0.03 | 0.03 | 1.56 | 0.79 | 0.50 | 0.25 | 0.29 | 1.03 |
| Cu | – | – | – | 0.10 | 0.14 | 0.38 | 0.00 | 0.40 | 0.59 | 0.17 | – | – | – | – | – | – | 0.10 | – | – | – | – | – | – | – | – | – | – | – | – | – | – | – |
| ∑oct | 5.70 | 5.67 | 5.78 | 5.81 | 6.02 | 5.70 | 5.64 | 5.65 | 5.66 | 5.62 | 3.01 | 3.01 | 2.84 | 2.78 | 2.82 | 2.91 | 2.76 | 2.89 | 2.84 | 2.77 | 2.76 | 3.00 | 3.00 | 2.00 | 2.00 | 2.04 | 8.86 | 8.21 | 8.24 | 8.24 | 8.31 | 8.27 |
| Ca | – | 0.05 | 0.17 | – | – | 0.10 | – | – | 0.02 | 0.02 | 0.03 | 0.03 | 0.02 | 0.03 | 0.02 | 0.01 | 0.04 | 0.02 | 0.02 | 0.01 | 0.02 | – | – | 0.05 | 0.05 | 0.05 | 0.17 | 0.12 | 0.25 | 0.08 | 0.17 | 0.08 |
| Na | – | – | – | – | – | – | – | – | – | – | – | – | – | – | – | – | – | – | – | – | – | – | – | – | – | – | – | – | – | – | – | – |
| K | 0.07 | – | – | – | – | 0.12 | – | – | – | – | 0.03 | 0.01 | – | – | 0.01 | 0.01 | – | – | – | – | – | – | – | 0.03 | 0.05 | 0.08 | – | 0.04 | – | – | – | – |
| Mg | – | – | – | – | – | – | – | – | – | – | – | – | – | – | – | – | – | – | – | – | – | 0.13 | 0.09 | 0.20 | 0.21 | 0.20 | – | – | – | – | – | – |
| ∑int | – | – | – | – | – | – | – | – | – | – | – | – | – | – | – | – | – | – | – | – | – | 0.26 | 0.18 | 0.54 | 0.58 | 0.58 | 0.34 | 0.29 | 0.50 | 0.16 | 0.33 | 0.16 |
| | *(14O, $Fe^{2+}$)* | | | | | | | | | | *(7O, $Fe^{2+}$)* | | | | | | | | | | | *(11O, $Fe^{3+}$)* | | | | | *(25O, $Fe^{2+}$)* | | | | | |

Average formula:

Chl$_2$ $K_{0.02}\,Ca_{0.04}\,(Si_{3.27}\,Al^{IV}_{0.73})_4\,(Mg_{3.23}\,Al^{VI}_{1.18}\,Fe^{2+}_{0.83}\,Ni_{0.26}\,Cu_{0.16}\,Mn_{0.02}\,Ti_{0.02})_{5.7}\,O_{10}\,(OH)_8$ *(n = 12)*

Srp $K_{0.02}\,Ca_{0.02}\,(Si_{1.93}\,Al^{IV}_{0.08})_{2.01}\,(Mg_{0.80}\,Al^{VI}_{0.30}\,Fe_{0.37}\,Ni_{1.36})_{2.83}\,O_5\,(OH)_4$ *(n = 11)*

Note: *afu*, atoms per formula unit; *Bd*, beidellite; *Chl*, chlorite; *n*, number of analyses; *Nnt*, nontronite; *Sp*, saponite; Srp, serpentine; $\sum oct$, sum of octahedral cations; $\sum int$, sum of interlayer cations; —, not detected.

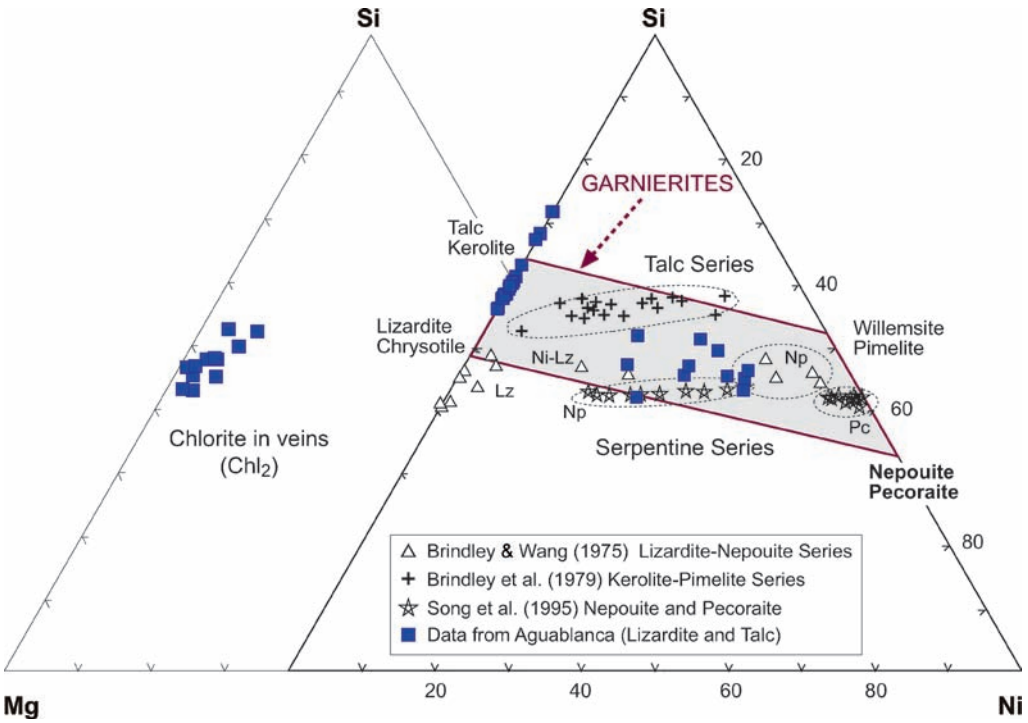


Fig. 8. Ni: Si: Mg ratios of chlorite, serpentine and talc in the Aguablanca weathering profiles. All data based on total cation valence of 28 with all Fe expressed as $Fe^{2+}$. Representative analyses of Ni-serpentine and Ni-talc from the literature are also plotted for comparison. Modified from Gleeson *et al.* (2003).
Note: *Lz*, lizardite; *Np*, nepouite; *Pc*, pecoraite.

at least two different mechanisms for their base-metal retention. Nickel and copper may occur: (i) bound to the structure of the sheet silicates, replacing $Mg^{2+}$ and $Fe^{2+}$ in octahedral sites, and (ii) as discrete $Cu^0$ or Ni-(Fe ± Cu) particles. Chlorite and serpentine are the main Cu- and Ni-bearing phases throughout the weathering profiles. However, they evidence differences in the distribution of these base-metals.

Chlorite, together with corrensite, smectite, and to a lesser extent vermiculite, phlogopite, and talc, all host Ni only within the layer structure, whereas Cu is favourably retained as metallic particles. Chlorite acts as the major Cu sink downprofile, and especially at open fractures ($Chl_2$). In contrast, serpentine accommodates large amounts of Ni in octahedral sites but negligible structural Cu, as determined by AEM data. Also, it seems to be the only clay mineral that host Ni-(Fe ± Cu)-rich particles, which may be the major sink for Cu in serpentine (as was initially determined by EDS). These observations point to an irregular, probably sequential base-metal retention process by sheet silicates at Aguablanca, which would depend not only on the host minerals but also on the prevailing weathering conditions.

## Ni and Cu incorporation

A common feature for all the sheet silicates that host significant Ni and Cu contents in Aguablanca is that they all reflect structural and chemical modifications, probably as a result of low-temperature hydrothermal and weathering processes. However, these deviations seem to be significant for the incorporation of Ni and/or Cu into these clay minerals.

Chlorite is progressively transformed from the stable *IIb* to the metastable *Ia* structure typical of hydrothermal chlorites in low-temperature environments (Brown & Bailey, 1962; Bailey, 1980). This chlorite might be a transitional form of various degrees of alteration reflected by the local transformation to smectite and minor vermiculite layers, and related mixed-layer minerals. This contamination could explain the interlayer cations, low octahedral sum, and high Si contents recorded in the chlorite analyses. This metastable stage has been widely documented for Ni-rich minerals composed of chlorite-like layers (defective chlorites) (Wiewióra & Szpila, 1975; Brindley, 1978; Noack & Colin, 1986). Similarly, chlorite in Aguablanca retains higher amounts of base-metals within the altered domains compared to the regular layers. In particular, corrensite and smectite in these domains host moderate structural Ni besides the native Cu particles. The suitability for the retention of base-metals of both the mixed structures and the smectite is well known (*e.g.*, Brindley & De Souza, 1975; Wiewióra & Szpila, 1975; Brindley, 1978; Nahon *et al.*, 1982; Paquet *et al.*, 1986; Decarreau *et al.*, 1987).

Serpentine is the most effective Ni-scavenger in the soil profiles and occurs closely associated with metastable chlorites ($Chl_2$, $Chl_3$). Therefore, it is restricted to the

subsurficial weathering domain over ore-grade areas of the *Gabbronorite Unit*. This nepouite was not observed associated with the clinochlore in the fresh gabbros ($Chl_1$), and also differs from the pure 1*T* Mg-lizardite (<0.08 wt% NiO) that develops in serpentinized ultramafic rocks in the deposit. This, together with the textural and compositional features observed, suggests a supergene origin for the nepouite. This could have precipitated from groundwater solutions or, perhaps, be derived from the solid transformation of chlorite through a late Ni-enrichment process, as has been reported for some serpentine minerals involved in the formation of *garnierite* (*e.g.*, Trescases, 1975; Milton *et al.*, 1983; Song *et al.*, 1995; Tauler *et al.*, 2007).

However, serpentine at the Aguablanca deposit resembles a rather pure nepouite. Some rejected analyses show a strong deficiency of $R^{2+}$ ions or silica excess probably caused by leaching at the edges of the clay particles, as has been widely reported for such Ni-rich phases (*e.g.*, Brindley & Hang, 1973; Uyeda *et al.*, 1973; Brindley & Wan, 1975; Brindley, 1978; Manceau & Calas, 1985; Pelletier, 1984). This process would remove not only soluble $R^{2+}$ ions and $OH^-$ from edge positions, but could also leave a silica residue. Colloidal silica is rare, but the adjacent arrangements of smectite layers could also explain the excess Si or the minor quantities of $Ca^{2+}$ or $K^+$ occasionally recorded. Such compositional deviations are inherent in Ni-rich serpentines and are certainly indicative of their relatively low stability.

### Occurrence of metal Cu and Ni-(Fe ± Cu) particles

*Copper particles*

The occurrence of native Cu particles in both di- and trioctahedral sheet silicates, analogous to those particles observed at Aguablanca, has been widely described in altered domains of porphyry copper deposits as a result of weathering of the Cu-mineralization (*e.g.*, Ilton & Veblen, 1988, 1993; Ahn *et al.*, 1997).

Metallic Cu may form in a wide range of pH, but it requires relatively low Eh conditions (from −0.5 to +0.5; *e.g.*, Williams, 1990), which is consistent with the weakly oxidized subsurficial levels in the Aguablanca weathering profiles. However, the occurrence of these Cu particles is always associated with phyllosilicates, and this suggests a reducing agent limited to the grain scale.

This supergene Cu-enrichment process has been satisfactorily explained in some Cu-bearing sheet silicates after the reduction of the $Cu^{2+}$ ions by the oxidation of the octahedrally coordinated $Fe^{2+}$ (*e.g.*, White & Yee, 1985; Ilton *et al.*, 1992; Markl & Bucher, 1997) according to the ideal reaction: $2Fe^{2+} + Cu^{2+} = 2Fe^{3+} + Cu^0$. Ferrous iron has probably also promoted the nucleation of native Cu in $Fe^{2+}$-bearing-sheet silicates at Aguablanca, as in the metastable chlorites and the subtly altered phlogopite. Thus, Cu particles appear preferentially within the altered interlayer regions of these phyllosilicates, where ($Fe^{3+}$ ± $Cu^{2+}$)-smectite and -vermiculite are formed. As suggested by Markl & Bucher (1997), the most important key to this process is probably the weathering (hydrolysis) of the sheet silicates involved in the Cu retention, which reduces the solubility of Cu. Therefore, the amount of Cu retained will be limited by the amount of oxidizable ferrosilicate.

*Nickel-rich particles*

The anhedral morphology of the Ni-rich particles described in Aguablanca, which are irregularly distributed along layers of nepouite, suggests their late origin correlated with the formation of this clay mineral.

Natural Ni-rich compounds occluded in, or trapped on sheet silicates have been always difficult to characterize due to their commonly complex composition, physical features and distribution throughout the sheets. This is the case of many pseudo-amorphous Ni-rich compounds and Ni-oxides and hydroxides reported in *garnieritic minerals* (*e.g.*, Ammou-Chokroum, 1972; Springer, 1974; Poncelet *et al.*, 1979). Alternatively, metallic Ni nanoparticles in sheet silicates have been also reported, but only after reduction treatments under variable temperature conditions and inert atmospheres (*e.g.*, Poncelet *et al.*, 1979; Ghesquière *et al.*, 1982; Vieira-Coelho *et al.*, 2000; Richard-Plouet *et al.*, 2007).

Nickel at Aguablanca, accompanied by subordinated Fe and Cu, could be forming intermetallic compounds in nepouite since other elements like oxygen or silica are not clearly included in their composition (as determined by EDS). The progressive growth of serpentine (at the expense of chlorite and in the presence of $Ni^{2+}$ after sulphides alteration), could have locally reduced Ni ions at the edges of the crystals forming these particles, which further enhance the potential for metal-retention in this type of hydrous silicates.

## Concluding remarks

During the exogenic cycle in the Aguablanca deposit, Ni and Cu are released through subsurficial illuvial horizons of the weathering profiles, where they occur largely associated with sheet silicates. $Ni^{2+}$ and $Cu^{2+}$ ions from groundwater solutions have variably occupied octahedral sites in the structure of the partially altered inherited sheet silicates and the newly formed clay minerals. Moreover, native Cu- or Ni-(Fe ± Cu)-particles formed selectively at the grain scale via reduction, reflecting the influence of the local weathering conditions once the sulphide mineralization is altered and base-metals leached.

The determination of metal-sorption mechanisms during weathering in mineral deposits arises as a very important target from both the environmental and the mining point of view. However, it requires a previous evaluation of the metal-bearing phases and the real distribution of base-metals within them. This work reports on the selective retention of Ni and Cu among sheet silicates in a natural clay-rich setting, and evidences the importance of the

newly formed metallic or intermetallic compounds, as these may represent a large part of the metals captured by sheet silicates. It contributes to the knowledge of the processes that allow natural retention of Ni and Cu in supergene conditions.

**Acknowledgements:** The authors would like to thank the staff from Rio Narcea Recursos SA for their assistance during the field works. Technical support from Dept. Edafología y Química Agrícola and CIC (UGR), and from SGIker (UPV/EHU) is gratefully acknowledged. Assistance from Drs. I. Yusta, M.M. Abad, I. Guerra, I. Nieto, and G. López was essential for this work. The authors thank the two anonymous reviewers for their valuable comments and Drs. Lattanzi and Oberhänsli for handling the manuscript. Helpful comments from J. Arostegui and professor C. Dorronsoro are also acknowledged. We also thank C. Laurin for revising the English text. Financial support was supplied by research projects CGL2007-66744-C02-01/BTE, CGL2005-00798/BTE (MEC), and IT-340-10 (UPV).

## References

Ahn, J.H., Xu, H., Buseck, P.R. (1997): Transmission electron microscopy of native copper inclusions in illite. *Clays Clay Miner*., **45**, 295–297.

Ammou-Chokroum, M. (1972): Contribution à la valorisation des ferrallites nickélifères de Nouvelle-Calédonie. Distribution minéralogique des éléments et étude de leur comportement au cours de la réduction solide-gaz des matériaux. Thèse, Université de Nancy, 170 p.

Bailey, S.W. (1969): Polytypism of trioctahedral 1:1 layer silicates. *Clays Clay Miner*., **17**, 355–371.

— (1980): Structures of layer silicates. *in* ''Crystal Structures of Clay Minerals and their X-Ray Identification'', G.W. Brindley & G. Brown, eds. Mineralogical Society of London, 1–123.

— (1988a): X-ray diffraction identification of the polytypes of mica, serpentine, and chlorite. *Clays Clay Miner*., **36**, 193–213.

— (1988b): Chlorites: structure and crystal chemistry. *Min. Soc. Am. Rev. Miner*., **19**, 347–403.

Barros de Oliveira, S.M., Trescases, J.J., Melfi, A.J. (1992): Lateritic nickel deposits of Brazil. *Mineral. Deposita*, **27**, 2, 137–146.

Brindley, G.W. (1978): The structure and chemistry of hydrous nickel-containing silicate and aluminate minerals. *Bull. BRGM* (II), **3**, 233–245.

Brindley, G.W. & De Souza, J.V. (1975): Nickel-containing montmorillonites and chlorites from Brazil, with remarks on schuchardite. *Mineral. Mag*., **40**, 141–152.

Brindley, G.W. & Hang, P.-T. (1973): The nature of garnierites- I. Structures, chemical compositions, and color characteristics. *Clay Miner. Bull*., **21**, 17–40.

Brindley, G.W. & Wan, H-M. (1975): Composition, structures and thermal behaviour of nickel-containing minerals in the lizardite-nepouite series. *Am. Mineral*., **60**, 863–871.

Brindley, G.W., Bish D.L., Wan, H.-S. (1979): Compositions, structures, and properties of nickel-containing minerals in the kerolite-pimelite series. *Am. Mineral*., **64**, 615–625.

Brown, B.E. & Bailey, S.W. (1962): Chlorite polytypism: I. Regular and semi-random one-layer structures. *Am. Mineral*., **47**, 819–850.

Byström-Brusewitz, A.M. (1975): Studies on the Li test to distinguish between beidellite and montmorillonite. *in* ''Proceedings of the 5th International Clay Conference'', S.W. Bailey, ed. Applied Publishers, Wilmette, IL, 419–429.

Casquet, C. (1980): Fenómenos de endomorfismo, metamorfismo y metasomatismo en los mármoles de la Rivera de Cala (Sierra Morena). Tesis Doctoral, Universidad Complutense de Madrid, 295 p.

Casquet, C., Galindo, C., Tornos, F., Velasco, F. (2001): The Aguablanca Cu-Ni ore deposit (Extremadura, Spain), a case of synorogenic orthomagmatic mineralization: isotope composition of magmas (Sr, Nd) and ore (S). *Ore Geol. Rev*., **18**, 237–250.

Colin, E., Nahon, D., Trescases, J.J., Melfi, A.J. (1990): Lateritic weathering of pyroxenites at Niquelandia, Goiás, Brazil: the supergene behaviour of nickel. *Econ. Geol*., **85**, 1010–1023.

Cornell, R.M. & Schwertmann, U. (1996): The iron oxides. Structure, properties, reactions, occurrence and uses. VCH Verlagsgesellschaft, Weinheim, 573 p.

Davis, J.R. (2001): Copper and copper alloys. American Society for metals. International Handbook Committee, 652 p.

Decarreau, A., Colin, F., Herbillon, A., Manceau, A., Nahon, D., Paquet, H., Trauth-Badeaud, D., Trescases, J.J. (1987): Domain segregation in Ni-Fe-Mg-smectites. *Clays Clay Miner*., **35**, 1–10.

Dinelli, E. & Tateo, F. (2001): Sheet silicates as effective carriers of heavy metals in the ophiolitic mine area of Vigonzano (northern Italy). *Mineral. Mag*., **65**, 121–132.

Elias, M., Donaldson, M.J., Giorgetta, N. (1981): Geology, mineralogy, and chemistry of lateritic nickel-cobalt deposits near Kalgoorlie, Western Australia. *Econ. Geol*., **76**, 1775–1783.

Ghesquière, C., Lemaître, J., Herbillon, A. (1982): An investigation of the nature and reducibility of Ni-hydroxy-montmorillonites using various methods including temperature-programmed reduction (TPR). *Clay Miner*., **17**, 217–230.

Gleeson, S.A., Butt, C.M.R., Elias, M. (2003): Nickel laterites: a review. SEG Newsletter. *Soc. Econ. Geosci*., **54**, 9–16.

Greene-Kelly, R. (1952): Irreversible dehydration in montmorillonite. *Clay Miner. Bull*., **1**, 221–227.

— (1953): Irreversible dehydration in montmorillonite. Part II. *Clay Miner. Bull*., **2**, 52–56.

Gustafsson, Å.B. (2004): Sorption and Weathering Properties of Naturally Occurring Chlorites. L Thesis, Royal Institute of Technology, Stockholm, Sweden, 62 p.

Hendry, D.A.F., Chivas, A.R., Reed, S.J.B., Long, J.V.P. (1981): Geochemical evidence for magmatic fluids in porphyry copper mineralization. Part II. Ion probe analysis of Cu contents of mafic minerals, Koloula igneous complex. *Contrib. Mineral. Petrol*., **78**, 404–412.

Ilton, E.S. & Veblen, D.R. (1988): Copper inclusions in sheet silicates from porphyry copper deposits. *Nature*, **334**, 516–518.

—,— (1993): Origin and mode of copper enrichment in biotite from rocks associated with porphyry copper deposits: a transmission electron microscopy investigation. *Econ. Geol*., **88**, 885–900.

Ilton, E.S., Earley III, D., Marozas, D., Veblen, D.R. (1992): Reaction of some trioctahedral micas with copper sulfate

solutions at 25°C and 1 atmosphere: an electron microprobe and transmission electron microscopy investigation. *Econ. Geol*., **87**, 1813–1829.

Koppelman, M.H. & Dillard, J.G. (1977): A study of the adsorption of Ni (II) and Cu (II) by clay minerals. *Clays Clay Miner*., **25**, 457–462.

Maksimović, Z. (1975): The isomorphous series lizardite-nepouite. *Int. Geol. Rev*., **17**, 1035–1040.

Manceau, A. & Calas, G. (1985): Heterogeneous distribution of nickel in hydrous silicates from New Caledonia ore deposits. *Am. Mineral*., **70**, 549–558.

—,— (1986): Nickel-bearing clay minerals: II. Intercrystalline distribution of Ni: an X-Ray absorption study. *Clay Miner*., **21**, 341–360.

Manceau, A., Charlet, L., Boisset, M.C., Spadini, L. (1992): Sorption and speciation of heavy metals on hydrous Fe and Mn oxides. From microscopic to macroscopic. *Appl. Clay Sci*., **7**, 201–223.

Marañés, A., Sánchez, J.A., De Haro, S., Sánchez, S.T., Del Moral, F. (1998): Análisis de Suelos. Metodología e interpretación. Universidad de Almería. Servicio de Publicaciones, 84 p.

Markl, G. & Bucher, K. (1997): Reduction of $Cu^{2+}$ in mine waters by hydrolysis of ferrous sheet silicates. *Eur. J. Mineral*., **9**, 1227–1235.

Meunier, A. (2007): Soil hydroxy-interlayered minerals: a re-interpretation of their crystallochemical properties. *Clays Clay Miner*., **55**, 4, 380–388.

Milton, C., Dwornik, E.J., Finkelman, R.B. (1983): Pecoraite, the nickel analogue of chrysotile, $Ni_3Si_2O_5(OH)_4$ from Missouri. *N. Jb. Miner. Mh*., **146**, 513–523.

Nahon, D., Paquet, H., Delvigne, J. (1982): Lateritic weathering of ultramafic rocks and the concentration of nickel in the western Ivory Coast. *Econ. Geol*., **77**, 1159–1175.

Nickel, E.H., Clout, J.F.M., Gartrell, B.J. (1994): Secondary nickel minerals from Widgiemooltha, Western Australia. *Mineral. Rec*., **25**, 283–291.

Noack, Y. & Colin, F. (1986): Chlorites and chloritic mixed-layer minerals in profiles of ultrabasic rocks from Moyango (Ivory Coast) and Angiquinho (Brazil). *Clay Miner*., **21**, 171–182.

Ortega, L., Lunar, R., García-Palomero, F., Moreno, T., Martín-Estévez, J.R., Prichard, H.M., Fisher, P. (2004): The Aguablanca Ni-Cu-GE Deposit, Southwestern Iberia: magmatic ore-forming processes and retrograde evolution. *Can. Mineral*., **42**, 325–350.

Paquet, H., Colin, F., Duplay, J., Nahon, D., Millot, G. (1986): Ni, Mn, Zn, Cr-smectites, early and effective traps for transition elements in supergene ore deposits. *in* ''Geochemistry of the Earth Surface and Processes of Mineral Formation'', R. Rodriguez-Clemente & Y. Tardy, eds. Consejo Sup Invest Cient, CNRS, Granada, Spain, 221–229 p.

Pelletier, B. (1984): Localisation du nickel dans les minerais ''garniéritiques'' de Nouvelle-Calédonie. *in* ''International Congress on Alteration Petrology'', D. Nahon ed., CNRS, Paris, *Sci. Géol*., **73**, 173–183.

— (1996): Serpentines in nickel silicate ore from New Caledonia. *in* ''Nickel ′96. Conference proceedings'', E.J. Grimsey & I. Neuss, eds., Kalgoorlie, 27–29 November 1996, Australian Institute of Mining and Metallurgy, Publication Series, Vol. **6/96**, 197–205.

Piña, R., Gervilla, F., Ortega, L., Lunar, R. (2008): Mineralogy and geochemistry of platinum group elements in the Aguablanca Ni-Cu deposit (SW Spain). *Mineral. Petrol*., **92**, 259–282.

Poncelet, G., Jacobs, P., Delannay, F., Genet, M., Gerard, P., Herbillon, A. (1979): Étude préliminaire sur la localisation du nickel dans une garniérite naturelle. *Bull. Minéral*., **102**, 379–385.

Quesada, C., Florido, P., Gumiel, P., Osborne, J., Larrea, F., Baeza, L., Ortega, C., Tornos, F., Sigüenza, J. (1987): Mapa Geológico Minero de Extremadura. Junta de Extremadura, Dirección General Industria, Energía y Minas, 131 p.

Richard-Plouet, M., Guillot M., Vilminot, S., Leuvrey, C., Estournès, C., Kurmoo, M. (2007): *hcp* and *fcc* Nickel Nanoparticles Prepared from Organically Functionalized Layered Phyllosilicates of Nickel (II). *Chem. Mater*., **19**, 865–871.

Río Narcea Recursos S.A.-Lunding Mining Corporation (2009): Technical Report on the Aguablanca Ni-Cu Deposit, Extremadura Region, Spain, 169 p.

Romeo, I., Lunar, R., Capote, R., Quesada, C., Dunning, G.R., Piña, R., Ortega, L. (2006): U–Pb age constraints on Variscan magmatism and Ni–Cu–PGE metallogeny in the Ossa–Morena Zone (SW Iberia). *J. Geol. Soc. London*, **163**, 837–846.

Schultz, L.G. (1964): Quantitative interpretation of mineralogical composition from X-ray and chemical data for the Pierre Shale. US. Geological Survey Professional Paper, 391-C, C1-C31. United States Government Printing Office, Washington, D.C.

Song, Y., Moon, H.-S., Chon, H.-T. (1995): New occurrence and characterization of Ni-serpentines in the Kwangcheon area, Korea. *Clay Miner*., **30**, 211–224.

Springer, G. (1974): Compositional and structural variations in garnierites. *Can. Mineral*., **12**, 381–388.

Suárez, S., Prichard, H., Velasco, F., Fisher, P., McDonald, I. (2010): Alteration of platinum-group minerals and dispersion of platinum-group elements during progressive weathering of the Aguablanca Ni-Cu deposit, SW Spain. *Mineral. Deposita*, **45**, 4, 331–350.

Tauler, E., Buen, H., Proenza, J.A., Galí, S., Melgarejo, J.C., Labrador, M., Marrero, N. (2007): Tres generaciones de serpentina en el perfil laterítico niquelífero del NW de Cuba. *Macla*, **7**, 110.

Thornber, M.R. & Wildman, J.E. (1984): Supergene alteration of sulphides, VI. The binding of Cu, Ni, Zn, Co and Pb with gossan (iron-bearing) minerals. *Chem. Geol*., **44**, 399–434.

Tornos, F., Casquet, C., Galindo, C., Velasco, F., Canales, A. (2001): A new style of Ni-Cu mineralization related to the magmatic breccia pipes in a transpressional magmatic arc, Aguablanca, Spain. *Mineral. Deposita*, **36**, 700–706.

Tornos, F., Galindo, C., Casquet, C., Rodríguez Pevida, L., Martínez, C., Martínez, E., Velasco, F., Iriondo, A. (2006): The Aguablanca Ni-(Cu) sulfide deposit, SW Spain: geologic and geochemical controls and the relationship with a midcrustal layered mafic complex. *Mineral. Deposita*, **41**, 737–769.

Trescases, J.J. (1975): L'évolution Géochimique Supergène des Roches Ultrabasiques en Zone Tropicale. Formation des Gisements Nickélifères de Nouvelle-Calédonie. Mémoire 78. ORSTOM, Paris, 259 p.

Uyeda, N., Hang, P.-T., Brindley, G.W. (1973): The nature of garnierites II. *Clays Clay Miner*., **21**, 41–50.

Velasco, F. (1976): Mineralogía y Metalogenia de los skarns de Santa Olalla (Huelva). Tesis Doctoral, Universidad de Bilbao, Spain, 290 p.

Vieira-Coelho, A.C., Ladrière, J., Poncelet, G. (2000): Nickel, iron-containing clay minerals from Niquelandia deposit, Brazil. 2.

Behaviour under reducing conditions. *Appl. Clay Sci*., **17**, 183–204.

Weiss, Z. & Durovic, S. (1983): Chlorite polytypism. II. Classification and X-ray identification of trioctahedral polytypes. *Acta Cryst*. B, **39**, 552–557.

Wells, M.A., Ramanaidou, E.R., Verrall, M., Tessarolo, C. (2009): Mineralogy and crystal chemistry of ''garnierites'' in the Goro lateritic nickel deposit, New Caledonia. *Eur. J. Mineral.*, **21**, 467–483.

White, A.F. & Yee, A. (1985): Aqueous oxidation-reduction kinetics associated with coupled electron-cation transfer from iron-containing silicates at 25°C. *Geochim. Cosmochim. Acta*, **49**, 1263–1275.

Wiewióra, A. & Szpila, K. (1975): Nickel-containing regularly interstratified chlorite-saponite from Szklary, Lower Silesia, Poland. *Clays Clay Miner*., **23**, 91–96.

Williams, P.A. (1990): Oxide Zone Geochemistry. Ellis Horwood Limited, England, 286 p.

*Received 7 June 2010*
*Modified version received 27 September 2010*
*Accepted 14 December 2010*